Preprint Cambridge Centre for Computational Chemical Engineering ISSN 1473 – 4273

Application of stochastic weighted algorithms to a multidimensional silica particle model

William J. Menz [1], Robert I. A. Patterson [2], Wolfgang Wagner [2], Markus Kraft [1]

released: 9 July 2012

[1] Department of Chemical Engineering
and Biotechnology
University of Cambridge
New Museums Site
Pembroke Street
Cambridge, CB2 3RA
United Kingdom

[2] Weierstrass Institute for
Applied Analysis and Stochastics
Mohrenstraße 39
10117 Berlin
Germany

Preprint No. 120

Keywords: stochastic weighted algorithms, silica, coagulation

Edited by
Computational Modelling Group
Department of Chemical Engineering and Biotechnology
University of Cambridge
New Museums Site
Pembroke Street
Cambridge CB2 3RA
United Kingdom

Fax: + 44 (0)1223 334796
E-Mail: c4e@cam.ac.uk
World Wide Web: http://como.cheng.cam.ac.uk/

Abstract

This paper presents a detailed study of the numerical behaviour of stochastic weighted algorithms (SWAs) using the transition regime coagulation kernel and a multidimensional silica particle model. The implementation in the SWAs of the transition regime coagulation kernel and associated majorant rates is described. The silica particle model of Shekar *et al.* (2012, *J. Aerosol Sci.* **44** 83–98) was used in conjunction with this coagulation kernel to study the convergence properties of SWAs with a multidimensional particle model. High precision solutions were calculated with two SWAs and also with the established Direct Simulation Algorithm. These solutions, which were generated using large number of computational particles, showed close agreement. It was thus demonstrated that SWAs can be successfully used with complex coagulation kernels and high dimensional particle models to simulate real-world systems.

Contents

1 Introduction

Population balance equations describe the dynamic processes controlling the growth and evolution of particles. Stochastic particle methods offer an attractive choice of solution method as they are capable of tracking high-dimensional systems and provide information about the history of individual particles. The Direct Simulation Algorithm (DSA)–introduced in [3]–was developed to solve the Smoluchowski coagulation equation through the technique of fictitious jumps and majorant kernels. Since then, it has been extended in a variety of forms, including the Linear Process Deferment Algorithm (LPDA) which accelerates the simulation of surface processes [21].

These stochastic particle methods have already been used in conjunction with DSA to model a number of physical systems; for example, the formation of soot [18, 19, 22, 29]; flame synthesis of silica [24, 30, 32] and titania [33, 36]; and the aerosol synthesis of silicon nanoparticles [15].

In direct simulation, every computational particle in the ensemble represents the same number of real particles. In basic implementations of DSA, coagulation events deplete the ensemble until there is only one computational particle remaining in the ensemble. To avoid this, the ensemble may be duplicated when it is below 50 % capacity [13]. Even when extended to avoid computational particle depletion, DSA produces statistically noisy estimates of the concentrations of physically rare particles and other associated quantities [2, 23]. This can only be overcome by computationally expensive changes in the numerical parameters [23].

To avoid these issues, weighted particle methods can be used [4, 12, 23, 27, 37]. These methods have been presented in various forms such as the Mass Flow Algorithm (MFA) [4, 6, 16, 17, 35] and the algorithms developed in [8, 38]. Stochastic weighted algorithms (SWAs) differ from direct simulation and constant-number methods in that coagulation events do not reduce the number of computational particles. Instead, simulated coagulations in the SWAs adjust the statistical weight that is attached to each computational particle. This statistical weight is proportional to the number of 'real' particles represented by the computational particle.

A recent paper gave a comprehensive review of present adaptations of SWAs [23]. It also gave the general formulation of weighted particle methods. This framework allowed for the development of general weighting rules which describe how the statistical weights are adjusted during coagulation. Further, it assumed a general form of the coagulation kernel and formulated this in terms of majorant techniques: an important method of reducing computational costs [3, 22].

The majority of previous studies of SWAs presented either used a simple spherical particle model [1, 2, 26] or a simple coagulation kernel for which an analytical solution to the population balance can be found [23, 38]. In one case, it was suggested that discrepancies with experimental results were a product of not using a coagulation kernel valid across the full range of Knudsen numbers [16].

A detailed study was presented of the numerical behaviour of a multidimensional silica particle model [31] whose coagulation process is approximated by transition regime coagulation. The paper investigated the convergence of key system properties (*e.g.* particle

number concentration) with respect to the choice of certain numerical parameters. Such work provides an ideal foothold from which to understand the numerical behaviour of weighted particle methods. It also allows for direct comparison of the convergence properties and computational efficiency of the DSA with weighted particle methods.

It has been previously identified that SWAs are particularly useful when extended to spatially inhomogeneous systems [7, 9, 20]. If stochastic methods are to be used to model real systems with more sophisticated particle models, the numerical behaviour of these methods must be investigated. A test problem using a silica particle model and the transition regime coagulation kernel will extend the numerical studies conducted in [31].

The structure of this paper is as follows. In §2, the stochastic particle method used to solve the population balance equation is outlined. §3 shows how to implement the stochastic weighted algorithm for the transition regime coagulation kernel, and §4 gives the numerical studies used to test this system. The efficiency and convergence of the SWAs is discussed in §5 and the paper is concluded with a critical analysis of these methods as well further avenues for research are suggested.

2 Model

A fully-coupled gas-phase and particle model is used to simulate the formation of silica from tetraethoxysilane. The kinetic model describing the gas-phase decomposition is described in [24, 30] and consists of 58 reversible gas-phase reactions among 27 chemical species.

The population balance describing the creation, removal and modification of particles is solved using a stochastic particle method. The particle model considered in the present work is the silica model defined in [30] (based-on [14, 28]), which uses a detailed *type-space* to capture particle structure and morphology.

2.1 Type-space

A detailed mathematical formulation of the particle model's *type-space* was given in [31], however a brief overview of its salient features is presented here. Particles are represented as:

$$P_i = P_i(p_1, \ldots, p_{n_i}, \mathbf{C}) \tag{1}$$

where particle P_i contains n_i primary particles p_x. The information describing the common surface area between two primary particles is stored in the lower-diagonal matrix $\mathbf{C}$. Each primary is described by variables η_{Si}, η_{O} and η_{OH}:

$$p_x = p_x(\eta_{\mathrm{Si}}, \eta_{\mathrm{O}}, \eta_{\mathrm{OH}}) \tag{2}$$

where η_{Si} is the number of silicon atoms, η_{O} is the number of oxygen (non-OH) atoms and η_{OH} is the number of OH units. As the particle model tracks the number of chemical units of each primary and the aggregate structure, it is able to provide detailed information about the nature of a single silica particle. This highly-dimensional particle model represents

a significant advance in sophistication over simple spherical particle or 'surface-volume' models.

2.2 Particle processes

In this model, particles may be created and changed through several different processes. The implementation of these processes in the framework of the stochastic weighted algorithm is described in §3.2.

Inception: The collision of two gas-phase $Si(OH)_4$ monomers yields a particle with an initial state given by $p_1(\eta_{Si} = 2, \eta_O = 1, \eta_{OH} = 6)$. This occurs through the reaction:

$$Si(OH)_4 + Si(OH)_4 \rightarrow P\left(p_1(\eta_{Si} = 2, \eta_O = 1, \eta_{OH} = 6), \mathbf{C}\right) + H_2O \tag{3}$$

where the newly-incepted particle is denoted by P. Their rate of formation is based-on the transition coagulation kernel:

$$R_{incep} = \frac{1}{2} K^{tr}\left(Si(OH)_4\right) N_A^2 C_{Si(OH)_4}^2 \tag{4}$$

where $K^{tr}\left(Si(OH)_4\right)$ is the transition kernel as applied to $Si(OH)_4$ monomers (discussed in §3.2), N_A is Avogadro's constant and $C_{Si(OH)_4}$ is the gas-phase concentration of $Si(OH)_4$.

Surface reaction: Surface reactions may occur when a $Si(OH)_4$ monomer reacts with an -OH site on the surface of a primary particle in a fashion analogous to inception. This alters the composition of the particle in the following manner:

$$P_i(p_1, \ldots, p_x, \ldots, p_{n_i}, \mathbf{C}) + Si(OH)_4 \rightarrow P_i(p_1, \ldots, p'_x, \ldots, p_{n_i}, \mathbf{C}') + H_2O \tag{5}$$

The rounding due to surface reaction ($\mathbf{C} \rightarrow \mathbf{C}'$) is discussed by Shekar et al. [31]. A primary p_x is uniformly selected and transformed according to:

$$p_x(\eta_{Si}, \eta_O, \eta_{OH}) \rightarrow p'_x(\eta_{Si} + 1, \eta_O + 1, \eta_{OH} + 2) \tag{6}$$

The rate of surface reaction is proportional to the concentration of $Si(OH)_4$ precursor and the number of OH sites on the particle surface:

$$R_{surf}(P_i) = A_{surf} \exp\left(-\frac{E_A}{RT}\right) \eta_{OH}(P_i) N_A C_{Si(OH)_4} \tag{7}$$

where A_{surf} and E_A are the gas-phase Arrhenius constants.

Sintering: Neighbouring primary particles may sinter with each-other according to the excess surface area decay formula popularised by Koch & Friedlander [11]:

$$\frac{\Delta C_{xy}}{\Delta t} = -\frac{1}{\tau_S(p_x, p_y)} \left(C_{xy} - S_{sph}(p_x, p_y)\right) \tag{8}$$

where C_{xy} represents the element of the common-surface matrix $\mathbf{C}$ describing the common surface area of the two primaries p_x and p_y, and $S_{\text{sph}}(p_x, p_y)$ is their equivalent surface area. In the present work, a viscous-flow model is used to describe the characteristic sintering time τ_S as a function of diameter and temperature. Here,

$$\tau_S(p_x, p_y) = A_S \min\left[d_{\text{pri},x}, d_{\text{pri},y}\right] \exp\left(\frac{E_S}{T}\left[1 - \frac{d_{\text{p,min}}}{\min\left[d_{\text{pri},x}, d_{\text{pri},y}\right]}\right]\right) \tag{9}$$

where A_S, E_S and $d_{\text{p,min}}$ are empirical constants obtained from model-fitting [30]. The degree of sintering is measured by the 'sintering level' parameter [28]:

$$s(p_x, p_y) = \frac{\frac{S_{\text{sph}}(p_x,p_y)}{C_{xy}} - 2^{-\frac{1}{3}}}{1 - 2^{-\frac{1}{3}}}. \tag{10}$$

where $S_{\text{sph}}(p_x, p_y)$ is the surface area of the sphere with volume equal to the sum of the primaries' volume.

When the sinter process is called, the sintering level s of the neighbouring primaries is first checked against the coalescence criterion. If the sintering level is greater than 0.95, the particles are merged; otherwise, the particles are sintered according equation (8) for time Δt_{sinter} with

$$\Delta t_{\text{sinter}} = t - t_{\text{last update}} \tag{11}$$

where $t_{\text{last update}}$ was the last time the sintering characteristics of the particle were updated. Sintering also results in the release of water, the amount of which, like surface reaction, is proportional to the particle's statistical weight.

Intra-particle reaction: The -OH units on the surface of a primary particle may also react with each other to release water. A particle is transformed by a intra-particle reaction as:

$$P_i(p_1, \ldots, p_x, \ldots, p_{n_i}, \mathbf{C}) \rightarrow P_i(p_1, \ldots, p'_x, \ldots, p_{n_i}, \mathbf{C}') + \text{H}_2\text{O} \tag{12}$$

In a similar vein to surface reaction, a primary p_x is uniformly selected and adjusted by:

$$p_x(\eta_{\text{Si}}, \eta_{\text{O}}, \eta_{\text{OH}}) \rightarrow p'_x(\eta_{\text{Si}}, \eta_{\text{O}} + 1, \eta_{\text{OH}} - 2) \tag{13}$$

The rate of intra-particle reaction is calculated for each particle such that the Si:O ratio tends to 1:2 as $t \rightarrow \infty$. It is mathematically described by the difference between the surface-reaction rate and the whole-particle sintering rate:

$$R_{\text{int}}(P_i) = R_{\text{surf}}(P_i) - \frac{\eta_{\text{OH}}(P_i)}{2\,S(P_i)}\left[\sum_{x,y=1}^{n_i} \frac{C_{xy} - S_{\text{sph}}(p_x, p_y)}{\tau_S(p_x, p_y)}\right] \tag{14}$$

The reader is referred to [31] for the derivation and explanation of this formula.

Coagulation: The collision and sticking of two silica particles is referred to as coagulation. The coagulation of particles P_i and P_j is represented by the following change to the particles' state:

$$P_i(p_1, \ldots, p_{n_i}, \mathbf{C}) + P_j(p_1, \ldots, p_{n_j}, \mathbf{C}) \rightarrow P_k(p_1, \ldots, p_{n_i}, p_{n_i+1}, \ldots, p_{n_i+n_j}, \mathbf{C}) \tag{15}$$

The matrix **C** is transformed to include the connectivity of the old particles and that of the new point-connection [31]. The rate of coagulation is calculated using the transition coagulation kernel, discussed in Section 3.2.

3 Development of stochastic weighted algorithms

In Stochastic Weighted Algorithms, computational particles are described by a type x_i and a statistical weight w_i. The physical concentration of particles of type x_i is given by w_i/V_{smp}. The x_i are a renaming of the P_i from the previous section to be consistent with previous articles which present mathematical formulations of stochastic coagulation processes [20, 23].

3.1 Linear particle processes

While the rate expressions of linear particle processes such as inception and surface reaction remain unchanged in this weighted particle method [23], the interaction of these with the gas-phase must be carefully considered. A process which removes one molecule of A from the gas-phase and release one molecule of B into the gas-phase can be written as

$$(x_i, w_i) + A \rightarrow (x_i', w_i) + B. \tag{16}$$

The amount of A removed (ΔC_A) and B (ΔC_B) added is proportional to the statistical weight of the particle w_i and the scaling factor, that is,

$$\Delta C_A = -\frac{w_i}{N_{\text{A}} V_{\text{smp}}} \tag{17}$$

where V_{smp} refers to the computational sample volume, and

$$\Delta C_B = \frac{w_i}{N_{\text{A}} V_{\text{smp}}}. \tag{18}$$

Note that the statistical weight w_i remains unchanged throughout this process. Particles are created in the population balance with weight $w_i = 1.0$ where inception occurs.

3.2 Coagulation process

Coagulation events in the SWA are asymmetric [4]. An ordered pair of particles (x_i, w_i) and (x_j, w_j) coagulate at rate $K(x_i, x_j)w_j$ such that

$$(x_i, w_i), (x_j, w_j) \rightarrow (x_i + x_j, \gamma(x_i, w_i, x_j, w_j)), (x_j, w_j). \tag{19}$$

The computational particle (x_j, w_j) is unaffected by the simulated coagulation event, but the new particle with index i is constructed using (x_j, w_j). This applies to the new type $x_i + x_j$ and the new statistical weight, which is calculated with the weight transfer function γ [23] and discussed further in §3.2.4.

In the stochastic simulation of a coagulation process, the total jump rate R for coagulation using the direct simulation algorithm is given by [22]:

$$R = \frac{1}{2}\sum_{i\neq j}^{N(t)} \frac{K(x_i,x_j)}{V_{\text{smp}}} \tag{20}$$

where $N(t)$ is the number of stochastic particles in the ensemble at time t. When a weighted particle method is used, the jump rate is given by $K(x_i,x_j)w_j$ and coagulation is no longer symmetric [23], so the total rate expression is modified to

$$R = \sum_{i\neq j}^{N(t)} \frac{K(x_i,x_j)w_j}{V_{\text{smp}}} \tag{21}$$

The function $K(x_i,x_j)$ represents the physics of the coagulation process and is dependent on characteristics of the particle pair and the chemical conditions of the surrounds. The transition kernel is a popular choice as it approximates the more detailed Fuchs Interpolation Formula and is valid across a wide range Knudsen numbers [10, 25]. It is given by the harmonic average of the slip-flow kernel $K^{\text{sf}}(x_i,x_j)$ and free-molecular kernel $K^{\text{fm}}(x_i,x_j)$

$$K^{\text{tr}}(x_i,x_j) = \left(\frac{1}{K^{\text{fm}}(x_i,x_j)} + \frac{1}{K^{\text{sf}}(x_i,x_j)}\right)^{-1}. \tag{22}$$

The implementation of the transition kernel within direct simulation is explained in detail in [22]. Of key importance is the use of majorants, which provide computationally efficient approximations of the true kernel such that $\hat{K} \geq K$. In the context of SWAs, the majorant kernel $\hat{K}$ is written

$$\hat{K}\left(x_i,w_i,x_j,w_j\right) = \hat{K}\left(x_i,x_j\right)w_j \tag{23}$$

To adapt the transition kernel to weighted methods, the majorant techniques of [23] are used. Provided the coagulation kernel satisfies

$$\begin{aligned}\hat{K}\left(x_i,w_i,x_j,w_j\right) \leq\ & h_1^{(1)}(x_i,w_i)\,h_2^{(1)}(x_j,w_j) + h_1^{(2)}(x_i,w_i)\,h_2^{(2)}(x_j,w_j) + \\ & \ldots + h_1^{(n_h)}(x_i,w_i)\,h_2^{(n_h)}(x_j,w_j),\end{aligned} \tag{24}$$

where $h_i^{(j)}$ is part of an upper bound for $\hat{K}$ and n_h is the number of terms in the factorised expression, the majorant rate can be factorised as

$$\sum_{i,j=1}^{N(t)} \hat{K} \leq \lambda_1^{(1)}\lambda_2^{(1)} + \lambda_1^{(2)}\lambda_2^{(2)} + \ldots + \lambda_1^{(n_h)}\lambda_2^{(n_h)}, \tag{25}$$

where

$$\lambda_l^{(k)} = \sum_{i=1}^{N(t)} h_l^{(k)}(x_i,w_i), \quad k,l = 1,2,\ldots,n_h. \tag{26}$$

The quantities $h_l^{(k)}(x_i,w_i)$ are stored in a binary tree which enables rapid calculation of the sums $\lambda_l^{(k)}$ [6, 23]. They are also used to select the pair of particles for a coagulation event: more information on such processes is given in [6]. To apply this formulation to the the transition kernel, it needs to be considered separately as its two components.

3.2.1 Free-molecular kernel

The free-molecular kernel is dominant for Kn $\gg 1$ [10]. In this regime, the full kernel takes the form

$$K^{\mathrm{fm}}(x_i,x_j) = 2.2\sqrt{\frac{\pi k_{\mathrm{B}} T}{2}}\left(\frac{1}{m_i}+\frac{1}{m_j}\right)^{\frac{1}{2}}(d_i+d_j)^2 \tag{27}$$

where k_{B} is Boltzmann's constant, T is the temperature and m_i and d_i are the mass and collision diameter of particle i, respectively. This is decomposed into its majorant rate form $\hat{K}^{\mathrm{fm}}(x_i,x_j)$ with $K^{\mathrm{fm}}(x_i,x_j) \leq \hat{K}^{\mathrm{fm}}(x_i,x_j)$ to allow for efficient jump rate calculation.

$$\hat{K}^{\mathrm{fm}}(x_i,x_j) = \alpha\left(\frac{1}{\sqrt{m_i}}+\frac{1}{\sqrt{m_j}}\right)\left(d_i^2+d_j^2\right) \tag{28}$$

where the constant α is given by

$$\alpha = 2.2\,k_{\mathrm{maj}}\sqrt{\frac{\pi k_{\mathrm{B}} T}{2}} \tag{29}$$

and k_{maj} is the majorant rate scaling factor ($k_{\mathrm{maj}} = 2.0$), necessary to satisfy the inequality $K^{\mathrm{fm}} \leq \hat{K}^{\mathrm{fm}}$ [5]. To calculate the total majorant rate, $\sum_{i\neq j}\hat{K}^{\mathrm{fm}}(x_i,x_j)w_j$ must be calculated and split into the individual jump terms. Using Equation (28), we obtain

$$\begin{aligned}
&\sum_{i\neq j}\hat{K}^{\mathrm{fm}}(x_i,x_j)w_j = \\
&\alpha\left\{(N(t)-1)\sum d_i^2 m_i^{-\frac{1}{2}}w_i + \left[\sum d_i^2\sum m_i^{-\frac{1}{2}}w_i - \sum d_i^2 m_i^{-\frac{1}{2}}w_i\right] + \right. \\
&\left.\left[\sum d_i^2 w_i\sum m_i^{-\frac{1}{2}} - \sum d_i^2 m_i^{-\frac{1}{2}}w_i\right] + \left[\sum d_i^2 m_i^{-\frac{1}{2}}\sum w_i - \sum d_i^2 m_i^{-\frac{1}{2}}w_i\right]\right\}
\end{aligned} \tag{30}$$

The indices are neglected here for clarity, however all sums act from $i = 1$ to $N(t)$. For the free-molecular kernel, there are four $\lambda_l^{(1)}\lambda_l^{(2)}$ terms, giving $n_h = 4$. Note that a $\sum d_i^2 m_i^{-\frac{1}{2}}w_i$ term is subtracted from the other terms to remove self-coagulations. The majorant jump rate of free-molecular coagulation is therefore given by

$$\hat{R}^{\mathrm{fm}} = \sum_{i\neq j}^{N(t)}\frac{\hat{K}^{\mathrm{fm}}(x_i,x_j)w_j}{V_{\mathrm{smp}}}. \tag{31}$$

3.2.2 Slip-flow kernel

After substitution of the Cunningham slip correction factor and the Knudsen number, the slip flow kernel is given by

$$K^{\mathrm{sf}}(x_i,x_j) = \beta_1\left(\frac{1}{d_i}+\frac{1}{d_j}+\beta_2\left[\frac{1}{d_i^2}+\frac{1}{d_j^2}\right]\right)(d_i+d_j) \tag{32}$$

where β_1 and β_2 are constants, the former expressed as

$$\beta_1 = \frac{2k_B T}{3\mu} \tag{33}$$

with μ is the gas viscosity; and the latter as

$$\beta_2 = 1.257(2\sigma) \tag{34}$$

where σ is the mean-free-path of gas molecules. The slip-flow kernel does not need a majorant due to its simple form [22]. Thus, the sum can be directly expanded:

$$\begin{aligned}
&\sum_{i\neq j} K^{\mathrm{sf}}(x_i,x_j)w_j = \\
&\beta_1 \left\{2(N(t)-1)\sum w_i + \left[\sum d_i \sum d_i^{-1} w_i - \sum w_i\right] + \left[\sum d_i w_i \sum d_i^{-1} - \sum w_i\right] + \right. \\
&\beta_2 \left((N(t)-1)\sum d^{-1} w_i + \left[\sum d_i \sum d_i^{-2} w_i - \sum d^{-1} w_i\right] + \right. \\
&\quad \left.\left.\left[\sum d_i w_i \sum d_i^{-2} - \sum d^{-1} w_i\right] + \left[\sum d_i^{-1} \sum w_i - \sum d^{-1} w_i\right]\right)\right\}
\end{aligned} \tag{35}$$

The jump rate of slip-flow coagulation is thus given by

$$R^{\mathrm{sf}} = \sum_{i\neq j}^{N(t)} \frac{K^{\mathrm{sf}}(x_i,x_j)w_j}{V_{\mathrm{smp}}}. \tag{36}$$

3.2.3 Particle selection algorithm

Equations (30) and (35) comprise the majorant rate expression for the 'weighted majorant transition kernel':

$$\hat{K}(x_i,x_j)w_j = \begin{cases} \sum_{i\neq j} \hat{K}^{\mathrm{fm}}(x_i,x_j)w_j & \text{if } \hat{R}^{\mathrm{fm}} < R^{\mathrm{sf}} \\ \sum_{i\neq j} K^{\mathrm{sf}}(x_i,x_j)w_j & \text{if } \hat{R}^{\mathrm{fm}} \geq R^{\mathrm{sf}} \end{cases} \tag{37}$$

In a similar vein to [5], these expressions can be thought of as sums of individual rate terms. For example, Equation (30) can be rewritten as:

$$\hat{K}^{\mathrm{fm}}(x_i,x_j)w_j = \hat{K}^{\mathrm{fm},1} + \hat{K}^{\mathrm{fm},2} + \hat{K}^{\mathrm{fm},3} + \hat{K}^{\mathrm{fm},4} \tag{38}$$

where, as an illustration, the first free-molecular jump rate term is given by:

$$\hat{K}^{\mathrm{fm},1} = \alpha(N(t)-1)\sum_{i=1}^{N(t)} d_i^2 m_i^{-\frac{1}{2}} w_i \tag{39}$$

Comparing Equation (30) to Equation (25), we see that each of these individual rate terms $\hat{K}^{(\mathrm{fm},i)}$ is composed of two parts $\lambda_1^{(\mathrm{fm},1)}$ $\lambda_2^{(\mathrm{fm},1)}$. These two terms are given by for $\hat{K}^{\mathrm{fm},1}$:

$$\begin{aligned}
\lambda_1^{(\mathrm{fm},1)} &= (N(t)-1) \\
\lambda_2^{(\mathrm{fm},1)} &= \sum_{i=1}^{N(t)} d_i^2 m_i^{-\frac{1}{2}} w_i
\end{aligned} \tag{40}$$

Table 1: *Particle selection properties for the 'weighted' transition kernel*

Term	Equation	Particle 1	Particle 2
FM1	$(N(t)-1)\sum d_i^2 m_i^{-\frac{1}{2}} w_i$	Uniform	$d_i^2 m_i^{-\frac{1}{2}} w_i$
FM2	$\sum d_i^2 \sum m_i^{-\frac{1}{2}} w_i - \sum d_i^2 m_i^{-\frac{1}{2}} w_i$	d_i^2	$m_i^{-\frac{1}{2}} w_i$
FM3	$\sum d_i^2 w_i \sum m_i^{-\frac{1}{2}} - \sum d_i^2 m_i^{-\frac{1}{2}} w_i$	$m_i^{-\frac{1}{2}}$	$d_i^2 w_i$
FM4	$\sum d_i^2 m_i^{-\frac{1}{2}} \sum w_i - \sum d_i^2 m_i^{-\frac{1}{2}} w_i$	$d_i^2 m_i^{-\frac{1}{2}}$	w_i
SF1	$2(N(t)-1)\sum w_i$	Uniform	w_i
SF2	$\sum d_i \sum d_i^{-1} w_i - \sum w_i$	d_i	$d_i^{-1} w_i$
SF3	$\sum d_i w_i \sum d_i^{-1} - \sum w_i$	d_i^{-1}	$d_i w_i$
SF4	$(N(t)-1)\sum d_i^{-1} w_i$	Uniform	$d_i^{-1} w_i$
SF5	$\sum d_i \sum d_i^{-2} w_i - \sum d_i^{-1} w_i$	d_i	$d_i^{-2} w_i$
SF6	$\sum d_i w_i \sum d_i^{-2} - \sum d_i^{-1} w_i$	d_i^{-2}	$d_i w_i$
SF7	$\sum d_i^{-1} \sum w_i - \sum d_i^{-1} w_i$	d_i^{-1}	w_i

which yields the following selection properties $h_1^{(\mathrm{fm},1)}$, $h_2^{(\mathrm{fm},1)}$:

$$\begin{aligned} h_1^{(\mathrm{fm},1)} &= 1 \\ h_2^{(\mathrm{fm},1)} &= d_i^2 m_i^{-\frac{1}{2}} w_i \end{aligned} \tag{41}$$

A selection property of 1 indicates uniform selection probability; that is, each computational particle has an equal chance for being selected, regardless of its physical properties. The coagulating partners i and j are selected according to the probabilities:

$$\frac{h_1^{(\mathrm{fm},1)}(x_i, w_i)}{\lambda_1^{(\mathrm{fm},1)}} \text{ and } \frac{h_2^{(\mathrm{fm},2)}(x_j, w_j)}{\lambda_2^{(\mathrm{fm},1)}} \tag{42}$$

The particle selection properties and partial sums for the remainder of the free-molecular and slip-flow kernels are summarised in Table 1.

3.2.4 Coagulation jump process

If a coagulation event is selected to occur, two particles must be chosen from the ensemble and physically joined. This is represented by Equation 19. The weight transfer functions $\gamma(x_i, w_i, x_j, w_j)$ define how the statistical weights are manipulated through such a process and are summarised in Table 2 [23].

The two best performing weight transfer functions (SWA1 and SWA3) from the family derived in [23] were selected for the numerical tests in this work.

In a stochastic coagulation process, two particles are first selected to coagulate. For direct simulation, the mass of the second particle is added to the first, and the 'old' second particle is deleted. As discussed in §1, the ensemble will eventually deplete if not somehow replenished. This is done by doubling the ensemble when the number of computational particles $N(t)$ falls below half of the maximum capacity $N_{\max}$. When using SWAs, the

Table 2: *Definition of the coagulation weight transfer functions.*

Name	Formula
SWA1	$w_i \frac{w_j}{w_i + w_j}$
SWA3	$w_i \frac{m_i}{m_i + m_j}$

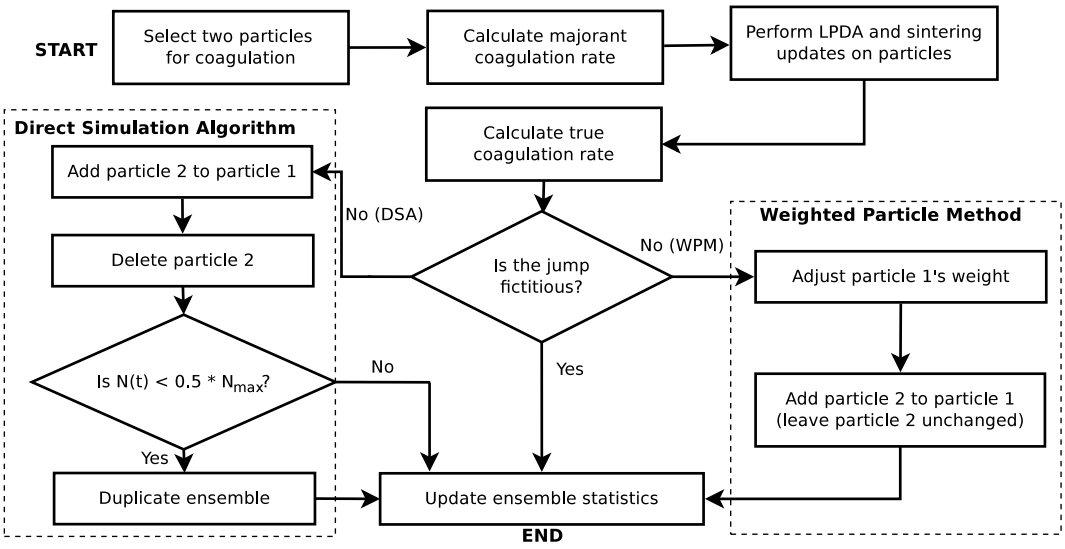

Figure 1: *Comparison of the coagulation process implemented in direct simulation algorithm and weighted particle methods.*

weight of the first particle is adjusted (using the functions in Table 2), the mass of the second particle is added to the first, and the second particle is left unchanged. As no particles are deleted, there is no need for a doubling algorithm. The ensemble properties cached in the binary tree structure (see [6, 23]) are updated at the end of the coagulation event. The complete process in which a coagulation event is handled is provided in Figure 1.

4 Numerical studies

A simple test-case was defined in [31] at which the numerical convergence studies were conducted. This case simulated a zero-dimensional batch reactor with 250 ppm of precursor (tetraethoxysilane, TEOS) in nitrogen bath gas. The temperature was held constant at 900 °C and a residence time of 0.8 s was chosen. The numerical parameters, model parameters and process settings used in the present work are summarised in Table 3.

Convergence of several functionals of the solution were studied; these are given along with their physical interpretations in Table 4. The convergence of these key process metrics was investigated in [31] by varying certain numerical parameters. In stochastic particle methods, such numerical parameters of interest include the maximum number of stochastic particles $N_{\max}$ and the number of simulation runs L.

Table 3: *Numerical and model parameters used in the present work.*

Description	Symbol	Value
Numerical parameters		
Number of splits	N_{splits}	100
Timestep	Δt	0.0015 s
Absolute error tolerance	ε_{a}	1.0×10^{-22}
Relative error tolerance	ε_{r}	1.0×10^{-4}
Maximum number of stochastic particles	N_{max}	64–131072
Number of runs	L	2048–1
Model parameters		
Maximum zeroth moment	$M_{0,\text{max}}$	1.55×10^{18} #/m^3
Sintering pre-exponential	A_{S}	1.1×10^{16} s/m
Sintering characteristic energy	E_{S}	1.2×10^{5} K
Sintering minimum diameter	$d_{\text{p,min}}$	4.4 nm
Surface smoothing factor	σ	1.0
Gas-phase parameters	-	[30]
Process settings		
Initial temperature	T	900 °C
Residence time	τ	0.8 s
Initial TEOS fraction	y_{TEOS}	250 ppm
Initial total pressure	P_i	1.0 atm

Table 4: *Summary of key process metrics (from Shekar et al. [32]) investigated in the present work.*

$m(t)$	Description	Formula
$M_0(t)$	Particle number concentration	$\frac{1}{V_{\text{smp}}} \sum w_i$
$F_{\text{V}}(t)$	Particle volume fraction	$\frac{1}{V_{\text{smp}}} \sum w_i V_i$
$\overline{n}(t)$	Mean number of primaries per particle	$\frac{1}{\sum w_i} \sum w_i n_i$
$\overline{d_{\text{col}}}(t)$	Mean collision diameter	$\frac{1}{\sum w_i} \sum w_i d_{\text{col},i}$
$\overline{d_{\text{pri}}}(t)$	Mean primary diameter	$\frac{1}{\sum w_i} \sum w_i d_{\text{pri},i}$
$\overline{s}(t)$	Mean sintering level	$\frac{1}{\sum w_i} \sum w_i s_i$

A high-precision solution was defined which used 131072 stochastic particles ($N_{\max} = 2^{17}$) and ten runs ($L = 10$). For simulations with multiple runs, the temporal evolution of a metric $m(t)$ is averaged over the number of runs:

$$\mu^{(N_{\max},L)}(t) = \frac{1}{L}\sum_{l=1}^{L} m^{(N_{\max},l)}(t) \tag{43}$$

The 99.9 % confidence interval is calculated using the variance and the central limit theorem:

$$c_{99.9}(t) = 3.29\sqrt{\frac{\frac{1}{L}\left[\sum_{l=1}^{L} m^{(N_{\max},l)}(t)^2\right] - \mu^{(N_{\max},L)}(t)^2}{L}} \tag{44}$$

Thus, the interval $I(t)$ in which there is a 99.9 % probability of finding the true solution of a metric for a simulation with given $N_{\max}$ and L is given by:

$$I(t) = \left[\mu^{(N_{\max},L)}(t) - c_{99.9}\ ,\ \mu^{(N_{\max},L)}(t) + c_{99.9}\right]\ . \tag{45}$$

The interval $c_{99.9}(t)$ is also used to measure the relative statistical error:

$$e_{\mathrm{r,stat}}(t) = \frac{c_{99.9}(t)}{\mu^{(N_{\max},L)}(t)} \tag{46}$$

5 Results

5.1 High-precision solution

Before investigating any useful convergence properties of the weighted methods, one must ascertain whether the solutions when using SWAs converge in the limit to those solutions when using direct simulation. Here, the high-precision solutions ($N_{\max} = 131072$, $L = 10$) are compared.

The particle size distributions (PSDs) predicted by the algorithms were first examined. As the silica model tracks primary particles, a PSD of the primary particles may be generated in addition to PSDs for the aggregates. The high-precision primary and collision PSDs are given for direct simulation and the weighted methods in Figure 2. These were generated using a Gaussian kernel density estimation procedure, and the normal distribution approximation to estimate the bandwidth [34].

It is evident that the SWA1 and SWA3 algorithms perfectly reproduce the PSD predicted by direct simulation. Further, SWA1/3 better resolve the large (>300 nm) and rare particles.

The metrics in Table 4 also provide a useful tool to examine agreement between algorithms. The temporal evolution of such metrics for the direct simulation and weighted algorithms is presented in Figure 3.

Again, the SWA1 and SWA3 algorithms produce trajectories with excellent agreement with those of DSA. The confidence intervals for these cases are typically too narrow

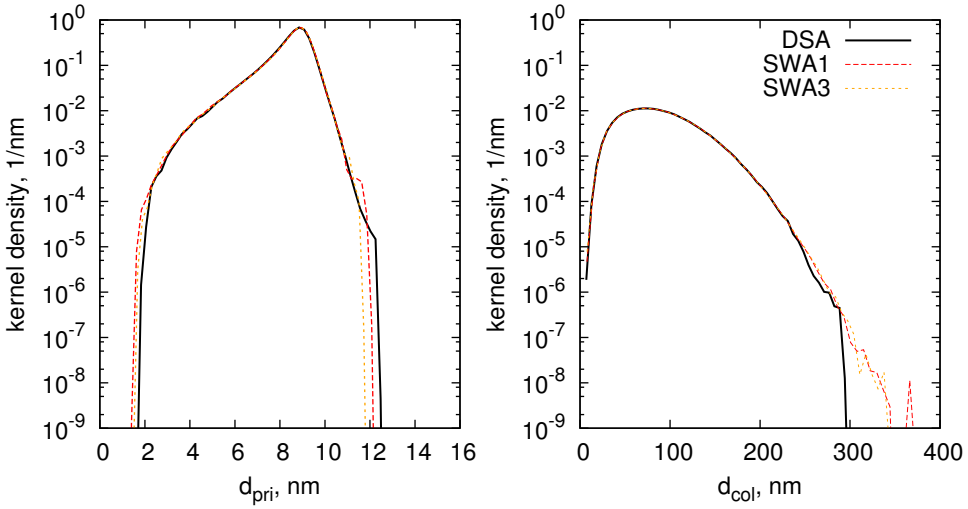

Figure 2: *PSDs predicted by the high-precision solutions at* $t = 0.8$ *s.*

to be observed here. It is clear that the SWAs' high-precision solutions are equivalent to those predicted through direct simulation, indicating that all algorithms approach the same solution in the limit as $N_{\max} \to \infty$.

5.2 Convergence of algorithms

When using stochastic particle methods, one must choose L such that the statistical uncertainty in the results is acceptably small. One must also chose $N_{\max}$ such that the systematic error appears close to zero, however in practice it may be chosen such that the differences between successive values of $N_{\max}$ are not statistically significant. The multidimensional silica particle model permits tracking of any number of functionals describing the particle size and morphology. Here, the convergence behaviour of these metrics is investigated.

The convergence studies reported here were conducted by varying $N_{\max}$ and L while holding their product $N_{\max} \times L$ constant at a value of 2^{17}. The relationship between the final average value of these functionals and $N_{\max}$ is given in Figure 4. The statistical errors associated with each of these values are depicted in Figure 5 and Figure 6.

Particle number concentration: The final value of the SWA solutions for particle number concentration M_0 (or zeroth moment) has lower systematic error than direct simulation.

Volume fraction: The volume fraction represents the ratio of total particle volume to gas volume. The SWAs achieve a solution within the confidence interval of the high-precision solution for $N_{\max} \geq 128$, indicating that they accurately predict the volume fraction for very few stochastic particles.

Mean number of primaries per particle: The mean number of primaries per particles is a measure of both the size of the aggregate and number of coagulation events. Figure 4 shows that much smaller aggregates are obtained when $N_{\max}$ is too low.

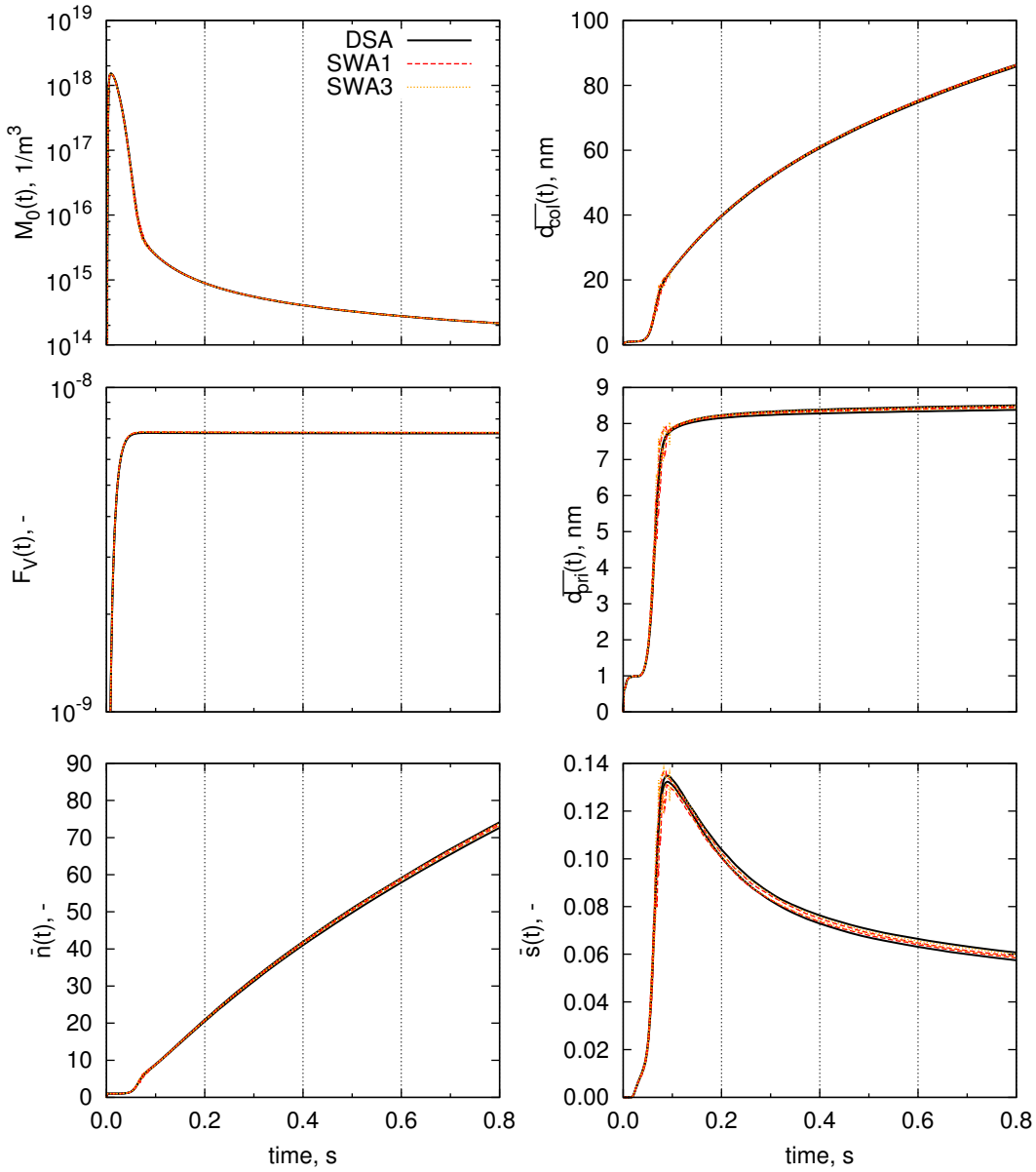

Figure 3: *Temporal evolution of Table 1's key metrics for the high-precision solutions using DSA and SWAs. The two lines show the upper- and lower-bound of the 99.9% confidence interval.*

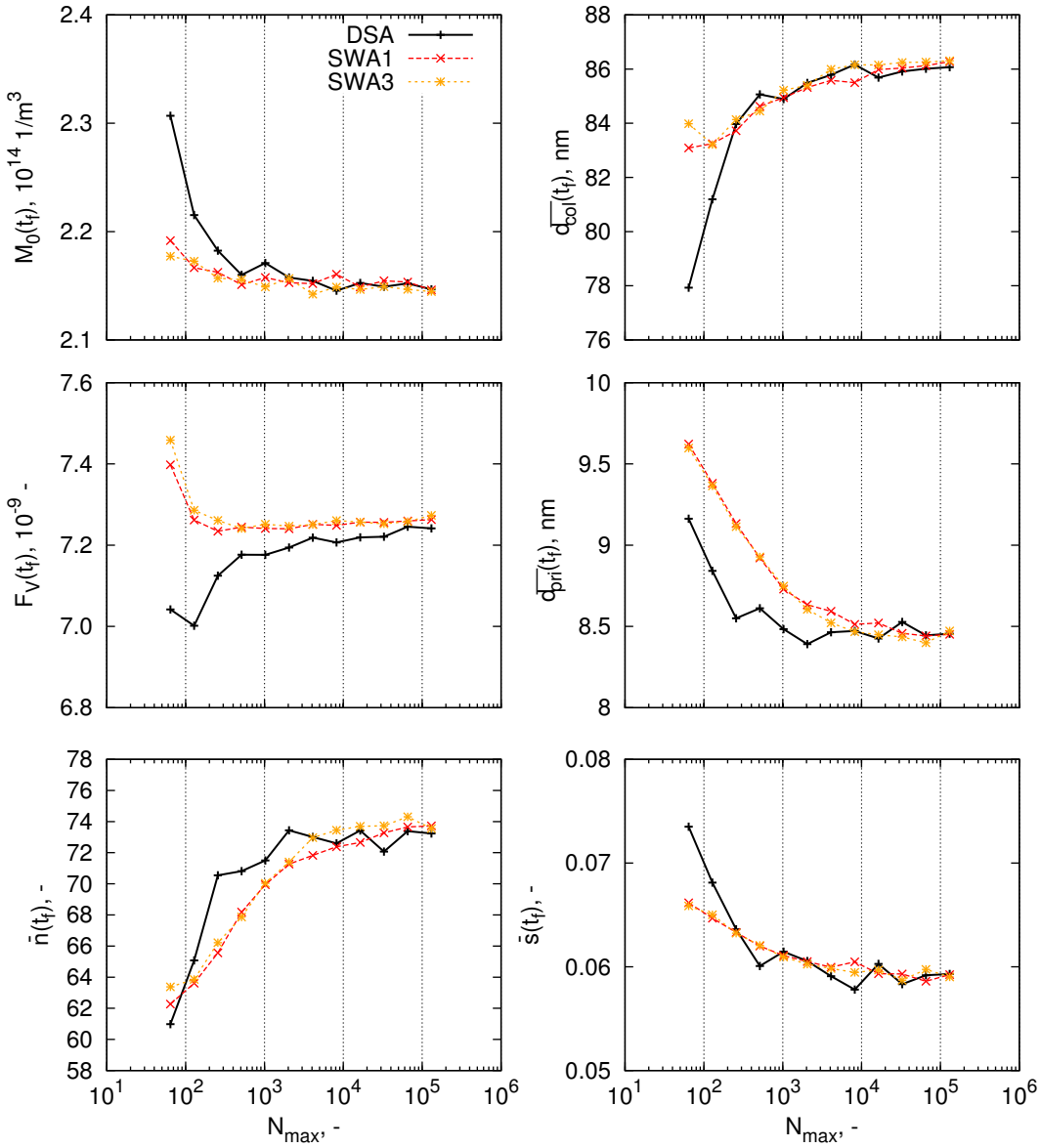

Figure 4: *Run-averaged values of the functionals studied (Table 4) at* $t = 0.8s$ *with* $N_{max} \times L = 2^{17}$.

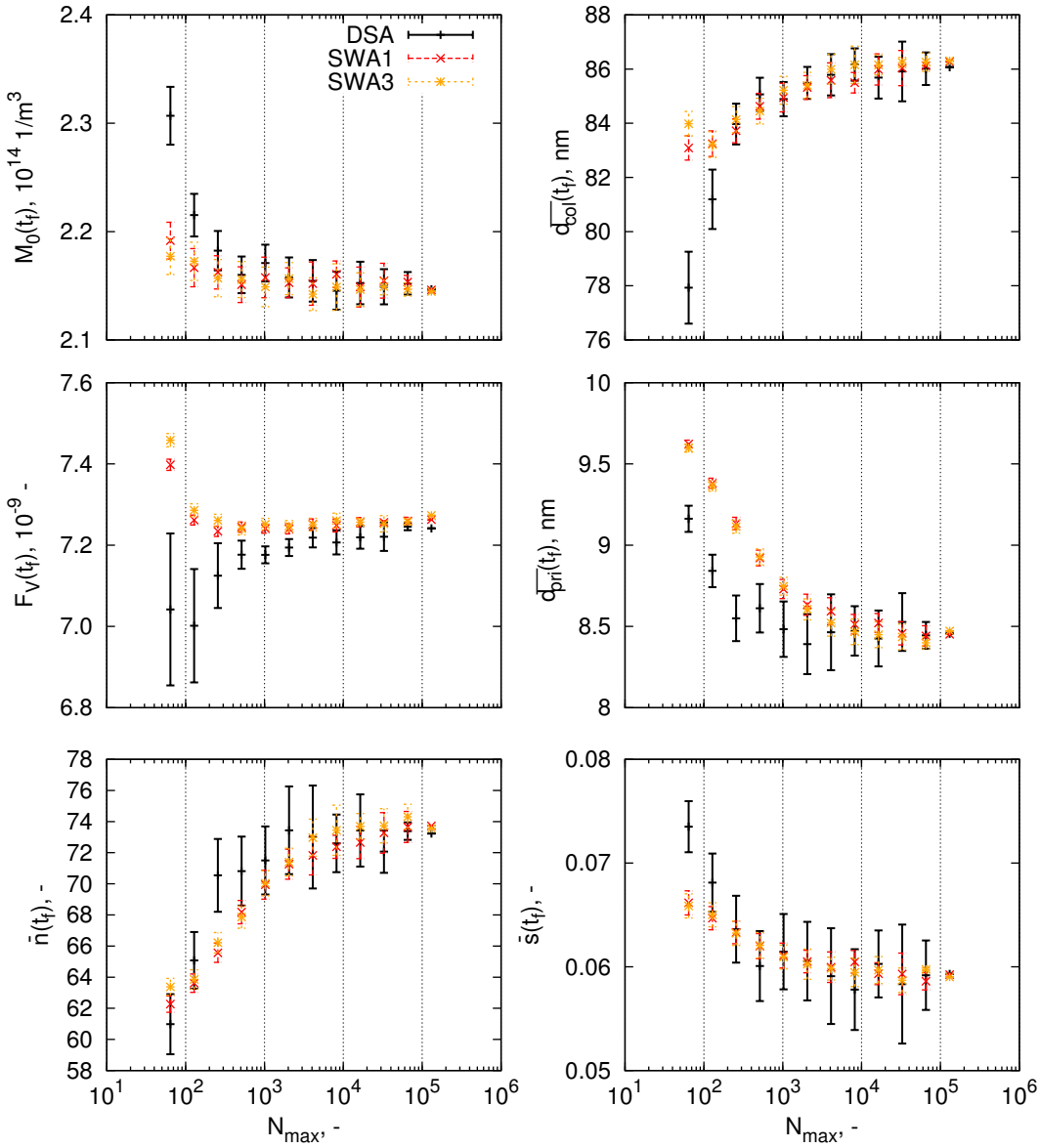

Figure 5: *Run-averaged values of the functionals studied (Table 4) and their corresponding confidence intervals at $t = 0.8s$ with $N_{max} \times L = 2^{17}$.*

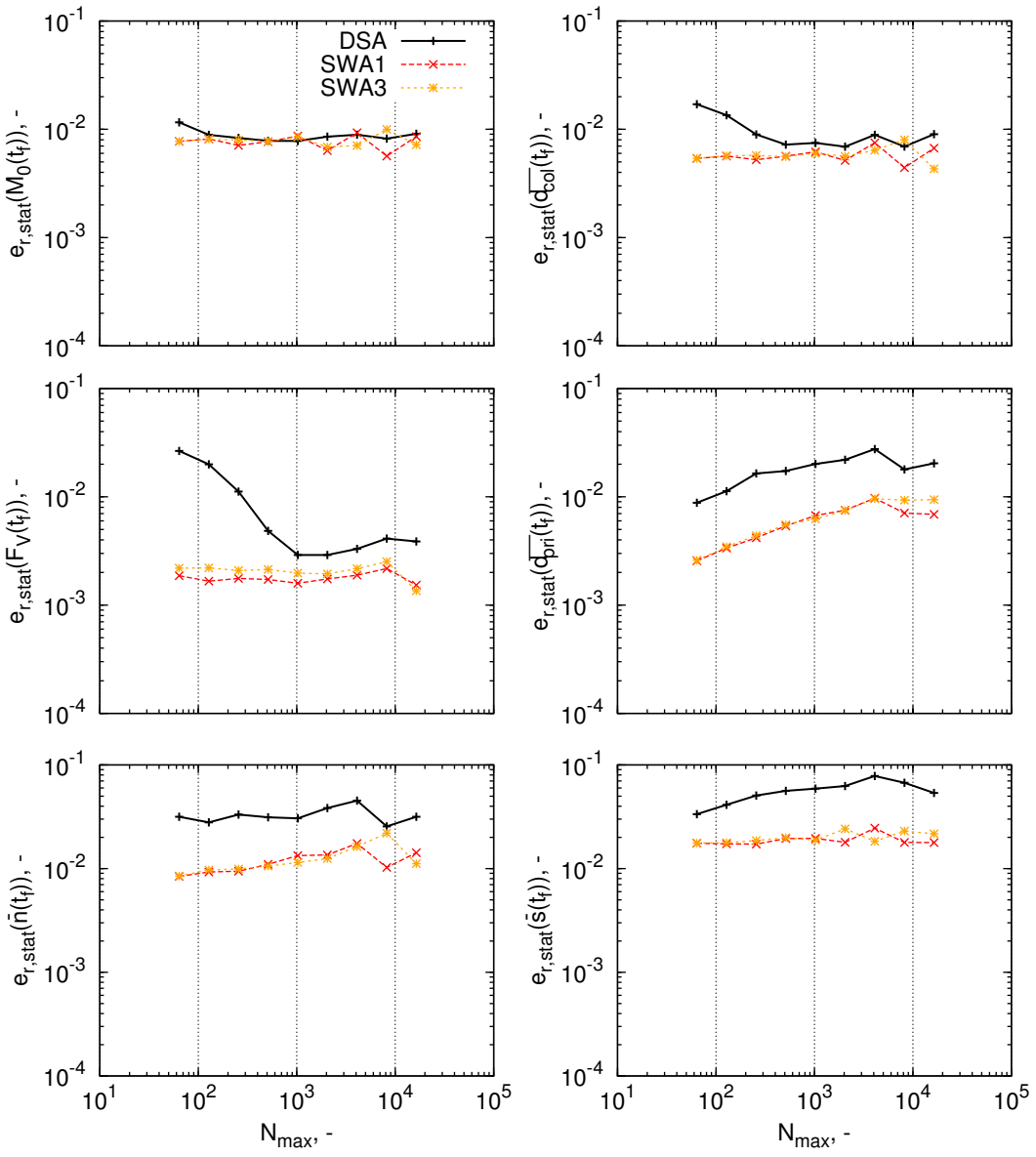

Figure 6: *Relative statistical error for Table 3's metrics with constant* $N_{max} \times L = 2^{17}$.

Mean collision diameter: The collision diameter $\overline{d_{\text{col}}}$ is an important property which characterises the size of an aggregate particle. SWAs appear to have better accuracy at lower N_{max}, but there is a common limit as N_{max} becomes large.

Mean primary diameter: The mean primary diameter $\overline{d_{\text{pri}}}$ estimates the average size of the primary particles which compose an aggregate. Curiously, despite SWAs predicting the final value of the collision diameter better than DSA, they have a larger systematic errror than DSA for fewer computational particles. This may be associated with SWAs preference towards larger particles (with larger primaries).

Mean sintering level: The mean sintering level is a measure of the extent to which the ensemble's particles are sintered. SWAs and DSA show similar convergence properties for this metric.

In summary, the weighted methods show convergence for fewer stochastic particles for M_0, F_{V}, $\overline{d_{\text{col}}}$, and the sintering level. Figure 5 demonstrates that the SWAs consistently have a smaller confidence interval than an equivalent DSA simulation with a given N_{max}, L. This is consistent with observations made in [23].

In any case, it is evident that Table 4's functionals satisfactorily converge to a stable value. For this system, a choice of $N_{\text{max}} \geq 16384$ would be recommended when using SWAs.

5.3 Computational efficiency

The computational time required to simulate the silica test system for a given N_{max}, L, or error is investigated in this section. These calculations were conducted on a SGI Altix Cluster with nodes composed of two 3.00 GHz quad core Intel Harpertown processors and 8 GB of RAM.

The computational times of the DSA and SWA simulations for increasing N_{max} are compared in Figure 7. Typically, a simulation with given N_{max} and $L = 1$ using SWAs required six to eight more times the CPU time than the equivalent DSA simulation. Further, it was observed that the time required per run increases approximately linearly with the maximum number of stochastic particles.

It is also no coincidence that the additional time required by the SWAs as compared to the DSA is proportional to the number of additional simulated coagulation events, which are shown in Figure 8. Firstly, as SWAs emphasise calculation of larger, rarer particles (e.g. [23] or Figure 2), more time on average is required to determine the extent of sintering (Equations (8) and (11)) of the ensemble's particles at the end of each timestep. Secondly, as SWAs always a full ensemble ($N(t) = N_{\text{max}}$), there are always more particles for which the process jump rates and sintering characteristics must be evaluated.

The additional numerical coagulation events that occur during SWA computations are a consequence of the redistributed statistical accuracy, that also reduces the variance of the studied metrics. This is depicted in Figure 6, where the confidence interval widths (or relative statistical error $e_{\text{r,stat}}$) for the metrics' final values are compared across algorithms. Generally, a constant confidence interval is obtained, with a few notable excep-

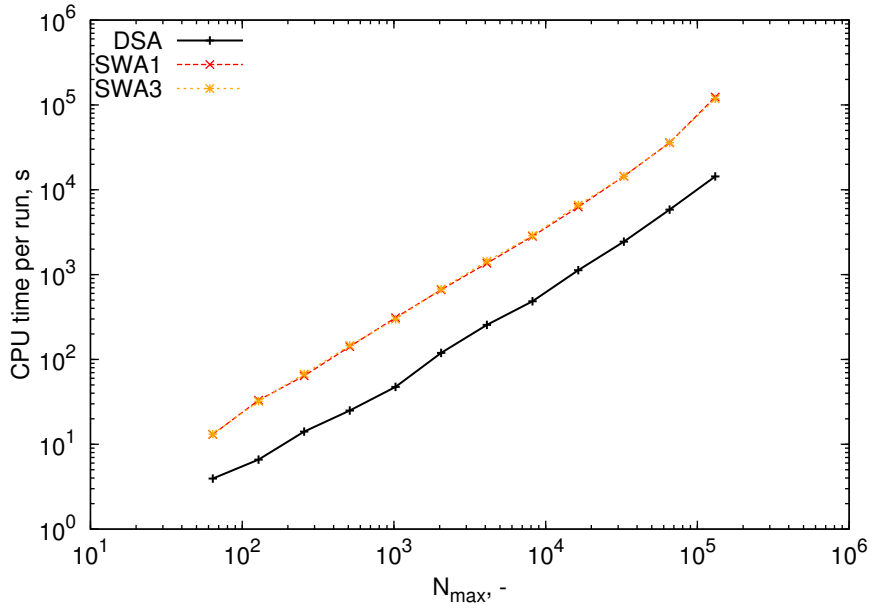

Figure 7: *Average CPU time required per run as a function of number of stochastic particles.*

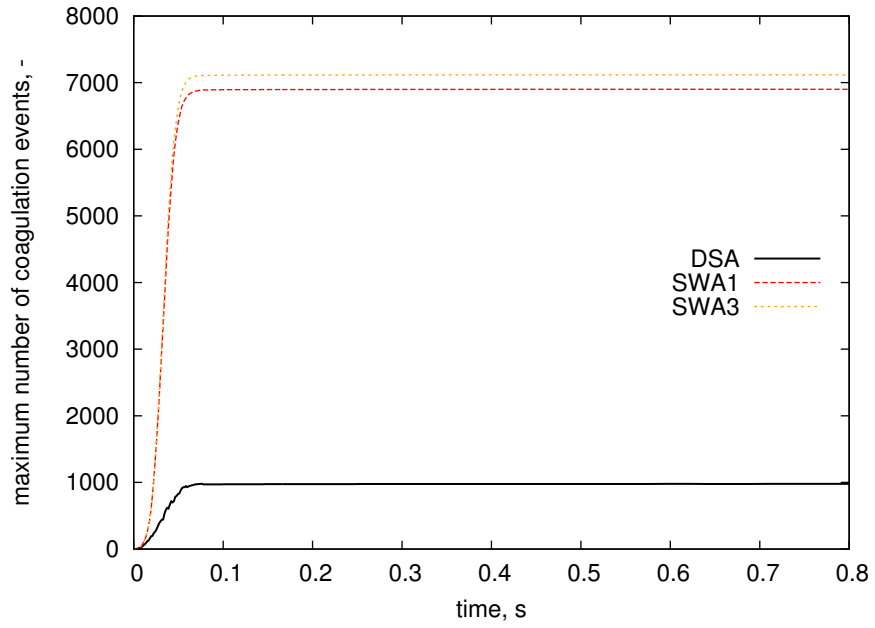

Figure 8: *Comparison of the maximum number of coagulation events undergone by particles for direct simulation and the SWAs for* $N_{max} = 131072$.

tions. Those metrics which show a steadily increasing or decreasing statistical errors correspond to the metrics whose final values (at $N_{\max}$ small) is significantly different ($\sim 10\%$) from the high-precision solution. That is, the presence of systematic error in the confidence interval when a simulation is unconverged affects the estimation of statistical error.

The size of the DSA confidence intervals with respect to the SWA intervals differs depending on the metric analysed. For the zeroth moment they are the same, however for primary diameter they differ by a factor of about 4. It is evident that the weighted methods offer superior variance reduction for all of the 'special' properties tracked in the multidimensional particle model.

6 Conclusions

This work has used majorant techniques to adapt the transition regime coagulation kernel to weighted particle methods. This is an important development if SWAs are to be used to solve real-world coagulation problems. This kernel is used in conjunction with a state-of-the-art multidimensional silica particle model to investigate the numerical behaviour of the population balance solution methodology.

Within the particle model, particles are described by the primary particles and their connectivity, which are in turn described by the number of Si, O and OH units of which they are composed. This permits tracking of many detailed features of the particles and particle ensemble through time.

Two SWAs (SWA1 and SWA3) were tested for convergence to direct simulation in the limit. Excellent agreement of all algorithms' high-precision solutions was obtained, indicating that the weighted algorithms are expected to converge to the direct simulation solution for sufficiently many stochastic particles.

The convergence of the functionals describing particle properties was investigated with respect to the maximum number of computational particles in the ensemble. SWAs generally achieved the correct value of these functionals for fewer stochastic particles than DSA, except in the calculation of number of primary particles and the primary diameter. For a calculation with a given number of stochastic particles and runs, the confidence intervals of the functionals were up to four times smaller, indicating that weighted algorithms studied here achieve better variance reduction than direct simulation. However, this comes at the cost of increased computational expense, with the algorithms requiring approximately seven times more CPU time per run than direct simulation.

The present work demonstrates that stochastic weighted algorithms can be successfully used to solve population balances with real-world coagulation kernels and complex particle models. This is particularly important for spatially inhomogeneous systems, where weighted methods offer practical and numerical advantages over direct simulation. A new majorant formulation of the transition kernel, as adapted to stochastic weighted algorithms is presented. A detailed numerical analysis of the convergence properties and efficiency of these methods was conducted, showing that weighted methods satisfactorily converge to a stable numerical solution.

7 Acknowledgements

W.J.M. acknowledges financial support provided by the Cambridge Australia Trust. M.K. is grateful for the suport of the Weierstrauss Institute for Applied Analysis and Stochastics (WIAS) in Berlin. The authors thank members of the Computational Modelling Group for their guidance and support.

References

[1] E. Debry, B. Sportisse, and B. Jourdain. A stochastic approach for the numerical simulation of the general dynamics equation for aerosols. *Journal of Computational Physics*, 184(2):649–669, 2003.

[2] R. DeVille, N. Riemer, and M. West. Weighted Flow Algorithms (WFA) for stochastic particle coagulation. *Journal of Computational Physics*, 230:8427–8451, 2011.

[3] A. Eibeck and W. Wagner. An efficient stochastic algorithm for studying coagulation dynamics and gelation phenomena. *SIAM Journal on Scientific Computing*, 22(3): 802–821, 2001.

[4] A. Eibeck and W. Wagner. Stochastic particle approximations for Smoluchoski's coagulation equation. *Annals of Applied Probability*, pages 1137–1165, 2001.

[5] M. Goodson and M. Kraft. An efficient stochastic algorithm for simulating nanoparticle dynamics. *Journal of Computational Physics*, 183(1):210–232, 2002.

[6] M. Goodson and M. Kraft. Simulation of coalescence and breakage: an assessment of two stochastic methods suitable for simulating liquid-liquid extraction. *Chemical Engineering Science*, 59(18):3865–3881, 2004.

[7] F. Guiaş. A stochastic numerical method for diffusion equations and applications to spatially inhomogeneous coagulation processes. In *Monte Carlo and Quasi-Monte Carlo Methods 2004*, pages 147–161. Springer, 2006.

[8] Z. Haibo, Z. Chuguang, and X. Minghou. Multi-Monte Carlo approach for general dynamic equation considering simultaneous particle coagulation and breakage. *Powder Technology*, 154(2-3):164–178, 2005.

[9] K. Kannenberg and I. Boyd. Strategies for efficient particle resolution in the direct simulation monte carlo method. *Journal of Computational Physics*, 157(2):727–745, 2000.

[10] A. Kazakov and M. Frenklach. Dynamic modeling of soot particle coagulation and aggregation: Implementation with the method of moments and application to high-pressure laminar premixed flames. *Combustion and Flame*, 114(3):484–501, 1998.

[11] W. Koch and S. K. Friedlander. The effect of particle coalescence on the surface area of a coagulating aerosol. *Journal of Colloid and Interface Science*, 140(2):419–427, 1990.

[12] A. Kolodko and K. Sabelfeld. Stochastic particle methods for Smoluchowski coagulation equation: variance reduction and error estimations. *Monte Carlo Methods Applied*, 9(4):315–339.

[13] F. Kruis, A. Maisels, and H. Fissan. Direct simulation Monte Carlo method for particle coagulation and aggregation. *AIChE Journal*, 46(9):1735–1742, 2000.

[14] P. Lavvas, M. Sander, M. Kraft, and H. Imanaka. Surface chemistry and particle shape: Processes for the evolution of aerosols in Titan's atmosphere. *The Astrophysical Journal*, 728:80, 2011.

[15] W. Menz, S. Shekar, G. Brownbridge, S. Mosbach, R. Körmer, W. Peukert, and M. Kraft. Synthesis of silicon nanoparticles with a narrow size distribution: a theoretical study. *Journal of Aerosol Science*, 44:46–61, 2012.

[16] N. Morgan, C. Wells, M. Kraft, and W. Wagner. Modelling nanoparticle dynamics: coagulation, sintering, particle inception and surface growth. *Combustion Theory and Modelling*, 9(3):449–461, 2005.

[17] N. Morgan, C. Wells, M. Goodson, M. Kraft, and W. Wagner. A new numerical approach for the simulation of the growth of inorganic nanoparticles. *Journal of Computational Physics*, 211(2):638–658, 2006.

[18] N. Morgan, M. Kraft, M. Balthasar, D. Wong, M. Frenklach, and P. Mitchell. Numerical simulations of soot aggregation in premixed laminar flames. *Proceedings of the Combustion Institute*, 31(1):693–700, 2007.

[19] R. Patterson and M. Kraft. Models for the aggregate structure of soot particles. *Combustion and Flame*, 151(1-2):160–172, 2007.

[20] R. Patterson and W. Wagner. A stochastic weighted particle method for coagulation–Advection problems. *SIAM Journal on Scientific Computing*, 34:B290–B311, 2012.

[21] R. Patterson, J. Singh, M. Balthasar, M. Kraft, and J. Norris. The linear process deferment algorithm: A new technique for solving population balance equations. *SIAM Journal on Scientific Computing*, 28(1):303, 2006.

[22] R. Patterson, J. Singh, M. Balthasar, M. Kraft, and W. Wagner. Extending stochastic soot simulation to higher pressures. *Combustion and Flame*, 145(3):638–642, 2006.

[23] R. Patterson, W. Wagner, and M. Kraft. Stochastic weighted particle methods for population balance equations. *Journal of Computational Physics*, 230:7456–7472, 2011.

[24] W. Phadungsukanan, S. Shekar, R. Shirley, M. Sander, R. West, and M. Kraft. First-principles thermochemistry for silicon species in the decomposition of tetraethoxysilane. *The Journal of Physical Chemistry A*, 113(31):9041–9049, 2009.

[25] S. Pratsinis. Simultaneous nucleation, condensation, and coagulation in aerosol reactors. *Journal of Colloid and Interface Science*, 124(2):416–427, 1988.

[26] N. Riemer, M. West, R. Zaveri, and R. Easter. Simulating the evolution of soot mixing state with a particle-resolved aerosol model. *Journal of Geophysical Research*, 114:D09202, 2009.

[27] S. Rjasanow and W. Wagner. A stochastic weighted particle method for the Boltzmann equation. *Journal of Computational Physics*, 124(2):243–253, 1996.

[28] M. Sander, R. West, M. Celnik, and M. Kraft. A detailed model for the sintering of polydispersed nanoparticle agglomerates. *Aerosol Science and Technology*, 43(10): 978–989, 2009.

[29] M. Sander, R. Patterson, A. Braumann, A. Raj, and M. Kraft. Developing the PAH-PP soot particle model using process informatics and uncertainty propagation. *Proceedings of the Combustion Institute*, 33(1):675–683, 2011.

[30] S. Shekar, M. Sander, R. Riehl, A. Smith, A. Braumann, and M. Kraft. Modelling the flame synthesis of silica nanoparticles from tetraethoxysilane. *Chemical Engineering Science*, 70:54–66, 2011.

[31] S. Shekar, W. Menz, A. Smith, M. Kraft, and W. Wagner. On a multivariate population balance model to describe the structure and composition of silica nanoparticles. *Computers and Chemical Engineering*, 43:130–147, 2012.

[32] S. Shekar, A. Smith, W. Menz, M. Sander, and M. Kraft. A multidimensional population balance model to describe the aerosol synthesis of silica nanoparticles. *Journal of Aerosol Science*, 44:83–98, 2012.

[33] R. Shirley, J. Akroyd, L. Miller, O. Inderwildi, U. Riedel, and M. Kraft. Theoretical insights into the surface growth of rutile TiO_2. *Combustion and Flame*, 158:1868–1876, 2011.

[34] B. Silverman. *Density estimation for statistics and data analysis*. Chapman & Hall/CRC, 1986.

[35] C. Wells, N. Morgan, M. Kraft, and W. Wagner. A new method for calculating the diameters of partially-sintered nanoparticles and its effect on simulated particle properties. *Chemical Engineering Science*, 61(1):158–166, 2006.

[36] R. West, M. Celnik, O. Inderwildi, M. Kraft, G. Beran, and W. Green. Toward a comprehensive model of the synthesis of TiO_2 particles from $TiCl_4$. *Industrial & Engineering Chemistry Research*, 46(19):6147–6156, 2007.

[37] J. Wu, W. Hsiao, Y. Lian, and K. Tseng. Assessment of conservative weighting scheme in simulating chemical vapour deposition with trace species. *International Journal for Numerical Methods in Fluids*, 43(1):93–114, 2003.

[38] H. Zhao, F. Kruis, and C. Zheng. A differentially weighted Monte Carlo method for two-component coagulation. *Journal of Computational Physics*, 229(19):6931–6945, 2010.